© 2017 Hefei Institutes of Physical Science, Chinese Academy of Sciences and IOP Publishing Printed in China and the UK

Plasma Sci. Technol. **19** (2017) 075101 (8pp) https://doi.org/10.1088/2058-6272/aa632e

Development of a radiographic method for measuring the discrete spectrum of the electron beam from a plasma focus device

Neda SHAMSIAN, Babak SHIRANI BIDABADI[1] and Hosein PIRJAMADI

Department of Nuclear Engineering, Faculty of Advanced Sciences and Technologies, University of Isfahan, Isfahan 8174673441, Iran

E-mail: b.shirani@ast.ui.ac.ir

Received 10 October 2016, revised 24 February 2017
Accepted for publication 25 February 2017
Published 24 May 2017

Abstract

An indirect method is proposed for measuring the relative energy spectrum of the pulsed electron beam of a plasma focus device. The Bremsstrahlung x-ray, generated by the collision of electrons against the anode surface, was measured behind lead filters with various thicknesses using a radiographic film system. A matrix equation was considered in order to explain the relation between the x-ray dose and the spectral amplitudes of the electron beam. The electron spectrum of the device was measured at 0.6 mbar argon and 22 kV charging voltage, in four discrete energy intervals extending up to 500 keV. The results of the experiments show that most of the electrons are emitted in the 125–375 keV energy range and the spectral amplitude becomes negligible beyond 375 keV.

Keywords: magnetized plasma, plasma focus, plasma diagnostics, electron beam, energy spectrum, x-ray dosimetry

(Some figures may appear in colour only in the online journal)

1. Introduction

The plasma focus (PF) device has proved to be an intensive source of pulsed electron beams [1–11]. In recent years, the electron beam of PF devices has been used in various fields, including thin-film deposition [12–14], material processing [15], and lithography [1]. The interaction of electron beam with the metal anode as a hard x-ray (HXR) source has also been proposed, mostly for radiography [16–20] and intra-operative radiation therapy [2–4] applications.

In this device, after the electrical breakdown of the working gas and the formation of a symmetric current sheath, the current sheath begins to move towards the open end of the electrodes due to the Lorentz force, thereby leading to the formation of a hot and dense plasma column. Owing to instabilities, this plasma column disrupts and generates pulsed intense electron and ion beams, which are emitted in opposite directions.

It is well known that HXR pulses are produced mainly by fast electron beams interacting with metal electrodes, but it is not known where and when such fast electron beams are generated and accelerated [21, 22]. Although there are many experimental results on the measurement of the electron beam produced by PF devices, a comprehensive mechanism is not yet available to explain the acceleration of electrons in this device [6–8]. One of the possible explanations is a hypothesis that some electrons are accelerated inside miniature plasma diodes, which can be formed due to magnetohydrodynamic instabilities of current filaments observed in PF discharges, and particularly inside pinch columns [22–24].

Experiments have revealed that the electron beam characteristics are independent of the energy stored in the capacitor bank [25]. Even in small PF devices, electrons having energies up to 1 MeV have reportedly been measured [6].

In most studies, the electron beam spectrum of PF devices is determined using a magnetic spectrometer [8–11]. Kwiatkowski *et al* directly measured the electron spectrum in the 40–800 keV range using a magnetic analyzer on PF-1000

[1] Author to whom any correspondence should be addressed.

[11]. Using a magnetic analyzer Patran *et al* measured the electron spectrum of a 3 kJ neon-filled PF device to be 30–660 keV [8, 9]. They also found that the energy of most electrons is below 200 keV, and that electrons with energy above 350 keV are negligible.

Some parameters of the electron beam were obtained using a Faraday cup. Stygar *et al* reported an electron energy distribution in the 20–500 keV range using an array of Faraday cups and a magnetic spectrometer [26]. They found that the energy distribution of the electrons conforms to the $E^{-3.5\pm0.5}$ power law.

Neong *et al* used a combination of the Faraday cup and Rogowski coil to measure the electron spectrum of a 2.2 kJ PF device [7]. The distribution range they came up with was 10–200 keV, with the most probable emission at 80–110 keV. They used a self-bias technique to find the distribution function of electron energy.

Pouzo *et al* [27] measured fast electron beams into a hollow anode of a small PF machine (2 kJ, 4 μF). The diagnostic method was a small Rogowski coil. In this way, they detected the electron beam pulses of about 10 ns width generated in the PF. The electron beam energy was measured through the time-of-flight of the electrons. The beams were found to be relativistic and their energies were into the range of HXR energy.

Neff *et al* measured the duration of high-energy electron beams from the PF by means of a Cerenkov detector. They found that the duration was less than 0.4 ns, pointing to beam currents of the order of the total discharge current [6].

Choi *et al* used a combination of a plasma optical light detector and a Cerenkov detector to give absolute timing between the maximum compression of the plasma and the production of a relativistic electron beam ($E > 180$ keV) in a 60 kV, 28 kJ Mather-type PF [28]. The observation of an electron beam prior to the first peak compression of the bulk plasma was reported.

In other research [29], Choi *et al* reported that the electron beam emission occurs in two periods: the first corresponded to the initial formation and disruption of the pinched plasma and terminated with the disruption of the plasma column, and the second period occurred after the breaking up of the focus plasma. The first period was characterized by high-energy electron beams, whereas in the second period the electron beams had lower average energies but higher currents. They found that the x-ray emission was closely related to the electron beam characteristics.

Schneider *et al* investigated the electron beam produced by a PF as a compact electron accelerator [30]. In that device, 5–20 ns electron beam pulses of several kA and particle energies of up to a few hundred keV were produced. The rms emittance of the electron beam was found to be 1288 mm-mrad.

Noll *et al* investigated the electron beam emitted from the PF by means of a Cerenkov detector streak camera equipment. The electron beam was measured to be strongly modulated with periods of about 25 ps [31].

In recent years, several studies have been conducted on the measurement of electron emissions in PF devices. Surala *et al* reported results of experimental studies on the pulsed electron beam of PF-360, the PF facility, by means of two different magnetic analyzers, which could record electrons in the vast 41–715 keV energy range [21, 22]. Their results showed relatively strong electron pulses in all measuring channels from 41–715 keV. Khan *et al* measured the electron beam of a 2.2 kJ PF device with a Faraday cup [32]. They concluded that the maximum electron beam emission was obtained at 1.7 mbar of argon. The maximum charge of the electron beam was 0.31 μC and the average energy was 500 keV, higher than the results recorded by other researchers.

Since extracting the electron beam from the chamber poses technical difficulties, electronic measurement instruments, which are typically complex and costly, must be installed inside the vacuum chamber. For this reason, it is difficult to directly measure the electron spectrum. The complexity of these experiments justifies the lack of experimental data on the electron beam characteristics in PF devices. Furthermore, it should be considered that the low-energy electrons are most likely to interact with the plasma or with the gas in the chamber, and high-energy electrons are emitted downwards and should go through the gas (and lose energy) to be measured. Therefore, due to the gas existing within the chamber, precise measurement of the electron spectrum by using the direct methods is inaccessible.

In some previous experiments, the Bremsstrahlung x-ray emitted from a target (the anode top surface in the PF device) was used as an indirect method to measure the electron beam spectrum. In PF devices, the dominant mechanism for the production of photons in the range of HXRs involves the collision of electrons with the anode, also known as the beam-target mechanism [17].

Paassen *et al* calculated the electron spectrum of a PF from an analysis of the HXR spectrum, which was measured by recording the tracks of the photoelectrons generated by x-ray photons in nuclear emulsions. Their work showed that the electron energy distribution extends up to 350 keV and conforms to the $E^{-3.3}$ power law [33].

Owing to the short duration of the electron emission in this device (50–150 ns), the Bremsstrahlung x-ray spectrum is often measured using passive dosimeters such as radiography film [18], nuclear track detectors [33], and thermoluminescent dosimeters [34] in a differential absorption technique. In this technique, the energy of the x-rays from any pulsed x-ray generator can be determined by unfolding the responses of the dosimeters behind filters of various materials with different thicknesses [35].

Raspa *et al* used a radiographic method to infer the HXR spectrum of a PF [18]. They performed differential absorption measurements using metals with different thicknesses.

In the present research, in accordance with the two cited works [18, 33], we used absorption foils, coupled with a radiographic film as the HXR detector to determine the electron spectrum of the PF device. In this method, the effect of the thick-target Bremsstrahlung x-ray photons (generated by the collision of the electrons with the anode surface) on a radiographic film was measured behind various absorption

foils, and the results were used to determine the electron spectrum, by using a matrix equation.

In a PF device, the electrons emitted from the pinch region have an angular distribution. However, it has been proved that the most intense and energetic electron beam is directed towards the anode surface [3–5]. Electron emission in the perpendicular direction (towards the film) is thus responsible for just a small portion of the total effect on the film and can be neglected. The presented method is intended as an investigation of the downward electron beam. The theory and validation procedure of this method are presented in the following section.

2. Theory and formulation

The method involves measuring the Bremsstrahlung x-ray using the radiography film in order to determine the electron spectrum in the PF device. The effect of an electron beam on any physical parameter, such as an absorbed dose and the intensity of the Bremsstrahlung x-ray, is equal to the sum of the effects of every single electron. Therefore, if we divide the energy spectrum of the electron beam and that of the Bremsstrahlung x-ray into n intervals, the spectral intensity of the Bremsstrahlung radiation in each interval would be equal to the sum of the Bremsstrahlung x-ray generated by the electrons of all n energy intervals.

This description can be written in the matrix form of equation (1):

$$\begin{bmatrix} X_1 \\ X_2 \\ \vdots \\ \vdots \\ X_n \end{bmatrix} = \begin{bmatrix} B_{11} & B_{12} & \cdots & B_{1n} \\ B_{21} & B_{22} & \cdots & B_{2n} \\ \vdots & \vdots & \cdots & \vdots \\ \vdots & \vdots & \cdots & \vdots \\ B_{n1} & B_{n2} & \cdots & B_{nn} \end{bmatrix} \times \begin{bmatrix} Y_1 \\ Y_2 \\ \vdots \\ \vdots \\ Y_n \end{bmatrix} \text{ or } X = B \times Y \quad (1)$$

where X is the matrix of the spectral intensities of the Bremsstrahlung spectrum, Y denotes the spectral intensities of the electron beam, and B is a coefficient matrix for the conversion of the electron spectrum to the Bremsstrahlung spectrum. Coefficient B_{ij} is the relative influence of electrons of the jth interval on the production of x-ray photons in the ith interval.

Furthermore, the absorbed dose on the film, behind each filter, is equal to the sum of the dose generated by the x-rays of all n energy intervals.

This can be described in the following matrix form of equation (2):

$$\begin{bmatrix} A_1 \\ A_2 \\ \vdots \\ \vdots \\ A_n \end{bmatrix} = \begin{bmatrix} D_{11} & D_{12} & \cdots & D_{1n} \\ D_{21} & D_{22} & \cdots & D_{2n} \\ \vdots & \vdots & \cdots & \vdots \\ \vdots & \vdots & \cdots & \vdots \\ D_{n1} & D_{n2} & \cdots & D_{nn} \end{bmatrix} \times \begin{bmatrix} X_1 \\ X_2 \\ \vdots \\ \vdots \\ X_n \end{bmatrix} \text{ or } A = D \times X \quad (2)$$

where A is the absorbed dose matrix behind n filters, which are measured using film dosimeters, and D is a coefficients matrix for conversion of the Bremsstrahlung spectrum to absorbed dose values. D_{ij} is the relative influence of x-rays of the jth interval on the absorbed dose of the film, behind the ith filter. The differences between the elements of matrix D are due to the dependence of the attenuation coefficient of the filter material and dose-energy response of the film on the energy of photons. Since matrix A is defined as the absorbed dose, attenuation coefficients, the energy to dose response function of the film, and other effective factors are considered in matrix D.

A matrix equation can be deduced from equations (1) and (2), to outline the relation between the electron spectrum and the absorbed dose of the Bremsstrahlung x-ray:

$$A = K \times Y \quad (3)$$

where $K = D \times B$ is the coefficients matrix for conversion of the electron spectrum to absorbed dose values.

Equation (3) shows that the absorbed dose on the film, behind each filter, is equal to the sum of the doses individually generated by the electrons of all n energy intervals. K_{ij} is the relative influence of the electrons of the jth interval on the production of the x-ray dose behind the ith filter.

Coefficients K_{11}–K_{nn} are complex functions of the B_{ij} and D_{ij} coefficients. Therefore, matrix K includes all the conversion factors from the electron beam to the absorbed dose. For a particular experiment setup, the K_{11}–K_{nn} coefficients are constant, and must be calculated using a proper simulation code. The calculations were performed with the Monte Carlo N-Particle (MCNP) code (see section 3.3). The calculation procedure includes n separate simulations. In each simulation, the absorbed dose of the x-ray behind all the n filters, generated by an electron beam having energies of jth interval, are calculated.

From equation (3), the absorbed dose behind the ith filter can be derived as follows:

$$A_i = K_{i1}Y_1 + K_{i2}Y_2 + \ldots + K_{ij}Y_j + \ldots + K_{in}Y_n. \quad (4)$$

Since the electrons have only the energies of the jth interval in each simulation, other spectral components of the electron spectrum are zero. Equation (4) can be described as the following:

$$A_i = K_{ij}Y_j. \quad (5)$$

Since all the results of the MCNP calculations are normalized to one particle of the electron source (i.e. $Y_j = 1$), we have $A_i = K_{ij}$ and A_i is the x-ray dose behind the ith filter generated by one electron of the jth interval. K_{1j}–K_{nj} are calculated from the results of this simulation, and this procedure is repeated for all electron energy intervals.

A matrix is said to be well conditioned if its condition number is close to one and ill conditioned if it is too large. The ratio of the largest to the smallest singular value in the singular value decomposition of the matrix is known as the condition number. Given a linear system of $A = K \times Y$, if K is an ill-conditioned matrix, the smallest changes in A or K create the biggest changes in the answer (Y). In other words, if an error occurs in the calculation of the matrix coefficients (e.g. there are statistical uncertainties about Monte Carlo calculations) or in the measurement of matrix A, this error is reflected in the results with very large factors. In this case, the

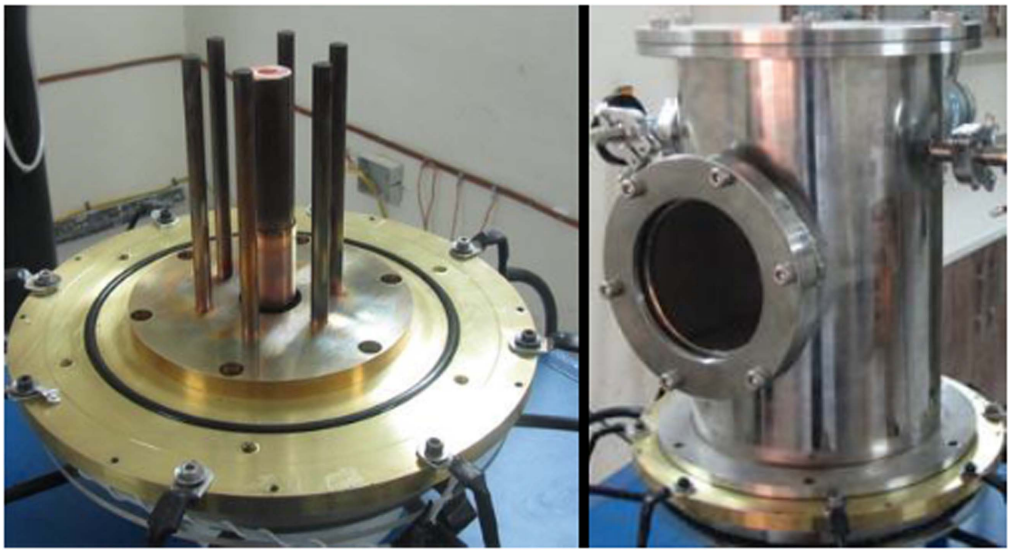

Figure 1. The PF device.

results are associated with large errors and are not reliable [36].

3. Experimental setup and methods

3.1. PF device

In this study, the energy spectrum of the electron beam emitted by a Mather-type PF device with 2.9 kJ stored energy was measured. This energy was supplied by a 12 μF capacitor at a charging voltage of 22 kV. A scheme of the electrodes and the discharge chamber of the device are shown in figure 1.

The discharge chamber comprises two coaxial copper electrodes and a Pyrex glass insulator across which the initial breakdown occurs. The inner and outer electrode diameters are 2.6 and 4 cm, respectively, and the Pyrex insulator is 6 cm in height. The axial spacing between the anode and cathode is 4 cm. A cylindrical vacuum vessel of stainless steel with 20 cm diameter and 32 cm height surrounds the electrode structure.

To evacuate the chamber, a rotary pump was used. To reduce the influence of gaseous impurities on the radiation output, fresh gas was injected after every four shots.

The depth of the spike on the current derivative signal determines the occurrence and the strength of the plasma focusing action in each shot. Current derivative signals were measured by a Rogowski coil and were registered by a 1 Gs s^{-1} digital oscilloscope.

3.2. Procedure of relative x-ray dose measurement

Agfa dental radiography film was used as the x-ray dosimeter. A set of filters made of lead, with deliberately selected thicknesses (68, 80, 148, and 320 μm), was used in these experiments. The best thicknesses completely covered the dynamic range of the film (from a low dose to the maximum allowed dose on the film), and made separable gray levels on the film. The x-ray film and the filters were pasted on the inner wall of the chamber of the PF device, at the same height of the anode's surface (perpendicular to the direction of the electron beam), at a distance of 9.75 cm from the anode top, as shown in figure 2.

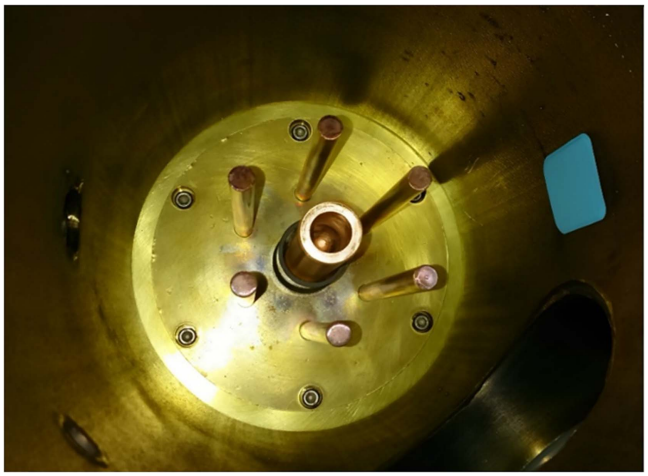

Figure 2. Position of the film and filters inside the PF chamber.

The films were all processed under the same laboratory conditions. The temperature and concentration of the film-processing solutions were fixed across all the experiments.

3.3. MCNP code

The MCNP code is a particle transport code based on the Monte Carlo method. The outputs of the MCNP code, such as flux, current, and dose of the particles, are normalized to be per source particle. A large number of particles are transported, from the source. The number of particles to be transported is determined by the NPS card in the input file of the code. The NPS parameter was 2×10^8 in the calculations of this research. The starting particle energy is determined by

the ERG card in the SDEF line of the input file. In the cases where the particles are not single energy, the energy of each starting particle is sampled from a given distribution. For example, in one of these calculations, 2×10^8 particles having 0–125 keV energies are transported from the source. In this case, uniform distribution was used for sampling. The results of the calculations are averaged over the 2×10^8 particles. In other words, the output of the MCNP code gives us the averaged x-ray dose generated by one electron of the source, having an energy range of 0–125 keV. Tally:F8 was used to calculate the absorbed dose in the film (matrix A).

3.4. Calculation of matrix K

The radiography film, as well as the lead filters, were placed in the chamber opposite the anode top surface, as shown in figure 2. This setup was simulated in the MCNP code, and matrices K ($n \times n$) and $D(n \times n)$ were calculated for different values of the matrix order, i.e. 'n'. The condition number of matrix K was as large as 10^4 for $n = 8$, while the condition number of matrix D was 130. Therefore, matrix K is the ill-conditioned one, whereas matrix D is somewhat well conditioned.

The condition number of about 10^4 means that the error will magnify by roughly a factor of 10^4. This might not be a problem if the error level is sufficiently low. But while the data come from the measurement of the x-ray dose, the error certainly will not be so low.

The condition number of matrix K depends on the setup of the experiment, and cannot be changed. Basically, the geometry and the setup are such that they lead to large condition numbers. Another approach to reducing the condition number involves reducing the order of the matrix. A higher-order matrix results in a higher magnification of errors; however, to determine the details of the spectrum, n should be as high as possible. Therefore, a compromise should be made between the resolution and the accuracy of the spectrum.

It was found that by selecting $n = 4$, the condition number is reduced to less than 10, and the electron spectrum can be measured with sufficient precision over four energy ranges.

3.5. Validation of the method

The validity of the method was ascertained using the MCNP Monte Carlo code. An electron source with an arbitrary spectrum, filters, and film was considered in the geometry of the PF device, and matrix K was calculated for this fixed geometry.

With the emission of the electrons from the source and their collision with the anode surface, the Bremsstrahlung x-ray is generated. Particle transport in the MCNP code includes all interactions that may occur for a particle (coulomb interaction, backscattering, etc). Thus, all of the possible processes are considered as part of the calculation of matrix K for the measurement of the electron spectrum.

By placing matrices A and K in equation (1), the energy spectrum of electrons (Y) emitted from the source was calculated. Figure 3 shows the hypothetical spectrum of electrons, as well as the spectrum calculated using the new method. The differences between the two spectra, at four intervals of energy, are not more than 7.5%, which certainly confirms the validity of the method.

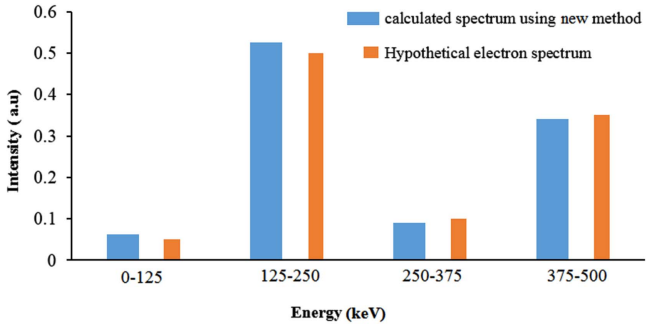

Figure 3. Hypothetical electron spectrum versus the calculated spectrum.

3.6. Error analysis

The uncertainties of the spectral amplitudes are due to the uncertainties of the measurements and their methods. In other words, when we solve the system $A = K \times Y$, matrices A and K both have uncertainties. In the case of matrix K, statistical uncertainties due to the Monte Carlo calculations should be considered. However, in the case of matrix A, uncertainties result from the measurement of the absorbed dose on the film behind filters. If the MCNP calculations were performed for a high enough number of source particles (the NPS parameter), and if the appropriate method of variance reduction was also used, the statistical uncertainties of the calculation results would be low enough (lower than 0.001% in our calculations) Thus, we can conclude that the uncertainties of the electron spectrum are predominantly generated by the measurements.

The standard deviation for any quantity U derived from measured variables x, y, z, … can be calculated from the following equation:

$$\sigma_U^2 = \left(\frac{\partial U}{\partial x}\right)^2 . \sigma_x^2 + \left(\frac{\partial U}{\partial y}\right)^2 . \sigma_y^2 + \left(\frac{\partial U}{\partial z}\right)^2 . \sigma_z^2 + \ldots \quad (6)$$

where $U = U(x, y, z, \ldots)$ represents the derived quantity.

Equation (6) is generally known as the error propagation formula. According to equation (3), matrix Y is derived from $Y = K^{-1} \times A$, where K^{-1} is the inverse of matrix K. Therefore, the ith entry of matrix Y is:

$$Y_i = K_{i1}^{-1} \times A_1 + K_{i2}^{-1} \times A_2 + K_{i3}^{-1} \times A_3 + K_{i4}^{-1} \times A_4 . \quad (7)$$

Using the error propagation formula, the standard deviation of Y_1 can be calculated as follows.

$$\sigma_{Y_i}^2 = (K_{i1}^{-1})^2 \times \sigma_{A_1}^2 + (K_{i2}^{-1})^2 \times \sigma_{A_2}^2 + (K_{i3}^{-1})^2 \times \sigma_{A_3}^2 + (K_{i4}^{-1})^2 \times \sigma_{A_4}^2 + A_1^2 \times \sigma_{K_{i1}^{-1}}^2 + A_2^2 \times \sigma_{K_{i2}^{-1}}^2 + A_3^2 \times \sigma_{K_{i3}^{-1}}^2 + A_4^2 \times \sigma_{K_{i4}^{-1}}^2 . \quad (8)$$

Since the standard deviations of the entries of matrix K are negligible in comparison with the standard deviations of the entries of matrix A, the last four terms of the right side of

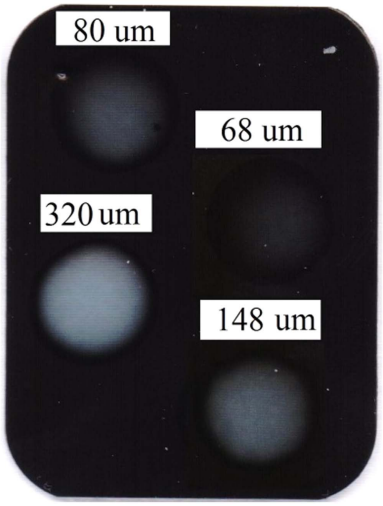

Figure 4. A sample of the irradiated films.

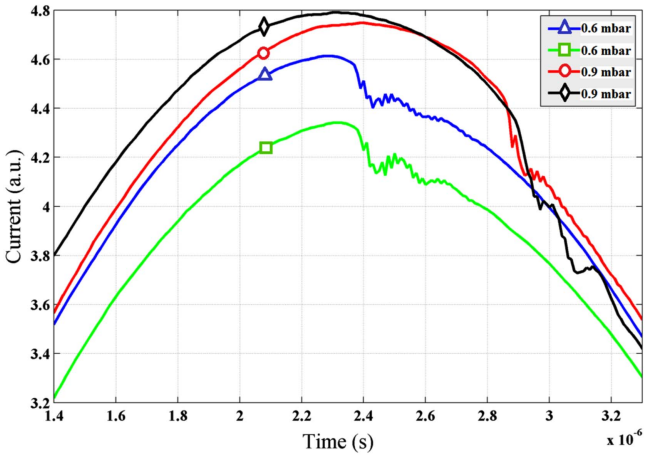

Figure 5. Current signals from four different shots ($V = 22$ kV, gas: argon).

equation (8) can be removed, and the equation (8) can be rewritten as:

$$\sigma_{Y_i}^2 = (K_{i1}^{-1})^2 \times \sigma_{A_1}^2 + (K_{i2}^{-1})^2 \times \sigma_{A_2}^2 + (K_{i3}^{-1})^2 \times \sigma_{A_3}^2 + (K_{i4}^{-1})^2 \times \sigma_{A_4}^2. \quad (9)$$

After digitizing an exposed film, the gray level of the film behind each filter was measured. The gray levels were converted to optical densities, which were then converted to the absorbed dose. The different pixels behind a filter would have different gray levels. This difference is due to the film processing and scanning procedure. Therefore, the dose value was averaged over 16 different pixels behind a filter. The sample standard deviation of the 16 values is the standard error of the dose value, and was less than 9% in all of the measurements (σ_{Aj} in equation (9)). This method is used to calculate the standard error of the dose value within a single lot of film. The experiment was repeated five times under similar conditions, using five different lots of film in order to reduce the standard error of the average dose value.

3.7. Other sources of dose to the film

The radiographic method is valid insofar as there are no sources of dose to the film, other than the Bremsstrahlung from the electrons impinging on the anode. Other possible sources of x-ray are the electrons impinging on other surfaces (besides the anode surface) and characteristic x-rays.

In a PF device, the electrons emitted from the pinch region have an angular distribution. However, the vast majority of the electrons are directed towards the anode surface [3–5], and electron emission in other directions is negligible. Therefore, the Bremsstrahlung emission that is generated by these electrons is too weak to have a measurable share in the total absorbed dose on the film.

The characteristic x-ray lines with the highest intensities in these experiments are K_α(2.96 keV) from argon and K_α (8.05 keV) from copper atoms. There are 8.05 or 8.9 keV photons of the K_β line of copper atoms attenuated by a factor of about 2.3×10^{-8} when penetrating the lead filter of 67.5 μm thickness. Therefore, the effect of the characteristic x-rays on the optical density of the film, even behind the thinnest filter, is certainly negligible.

In the cases where the anode of the device is made of a high-atomic-number element, such as tungsten ($Z = 74$, $K_\beta = 67$ keV), more energetic and characteristic x-rays can easily reach the film, and affect its final optical density. However, it should be considered that most devices have copper anodes, because of the high electrical conductivity of copper.

4. Results and discussion

Due to the statistical property of the output radiation of the PF device, the energy spectrum of the electron beam might be different even in experiments under nearly similar conditions. The accumulated spectrum of a large number of shots is much more predictable than the spectrum of a single shot. A higher number of shots means a lower standard deviation of the results. Therefore, each film was irradiated with four successful shots under similar conditions, and this experiment was repeated five films to obtain an average of the electron spectrum under those conditions. A sample of the irradiated films is shown in figure 4. If the dose values on the film, behind all the filters, are in the dynamic range of the film (in its characteristic curve), there will be a linear relation between the optical densities and the dose values. Therefore, the effect of four shots on the film is the sum of the effects of those shots.

The evidence that confirms the occurrence of a successful pinch is a sharp spike in the current signal. Figure 5 shows a sample of the current signals of four successful shots.

The operational conditions of the device were selected so that the strongest plasma pinch is reached. The optimum conditions for this device, working with argon, were experimentally determined to be 0.6 mbar of argon and 22 kV charging voltage. How the normalized energy spectrum of the electron beam of the device was calculated is shown in

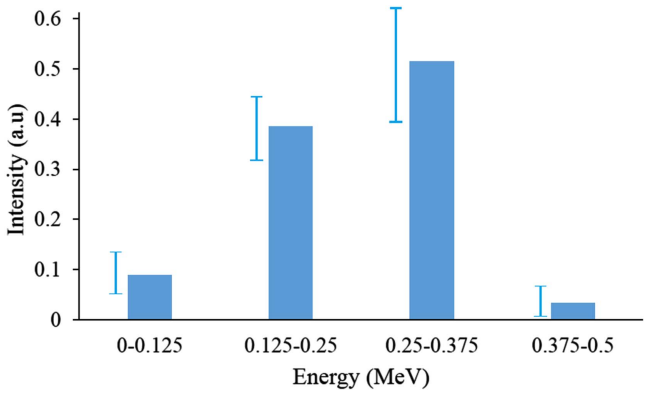

Figure 6. Electron energy spectrum of the device at 0.6 mbar, 22 kV working in argon.

figure 6. To be more precise, this is the electron spectrum from four shots of the PF device, under similar conditions.

About 50% of the emitted electrons have energies in the 250–375 keV range, and more than 88% of the electrons are emitted with energies between 125 and 375 keV. The spectral amplitude is very small above 375 keV. This confirms what Pattran *et al* found at high energies. They found that the intensity of electrons with energies higher than 350 keV is negligible in a similar 3 kJ device [8]. Passen *et al* also showed that the electron energy spectrum extends up to 350 keV [33]. At low energies, our method underestimates the spectrum compared to other works [7, 8]. Some of the differences may have resulted from the differences in the energy of the device, working gas, pressure, and the geometry of the electrodes. However, the considerable diversity of the results of the various papers is evidence that none of the presented methods are completely reliable for all the energies.

The uncertainties of the electron spectrum for each energy range were calculated in the form of relative standard deviations, or σ_{Y_i}/Y_i from the mean value using equation (9). Relative standard deviations were calculated to be 17%, 11%, 13%, and 78% for the spectrum in figure 6. The error bars on the spectrum also indicate uncertainties. There is a considerable overlap between the two strong components of the spectrum. However, it can be concluded that the 250–375 keV component is the strongest one.

Four data points as the final results of the electron spectrum measurement is rather scarce. However, this gives general information about the behavior of the spectrum, which will be valuable for industrial applications of the PF electron beam. Apart from the simplicity of the new method, the spectrum can be measured with more spectral components (more than four) if matrix K is calculated at higher orders (five, six, or more) with acceptable condition numbers.

Our calculations showed that matrix K is an ill-conditioned one, while matrix D is well conditioned. Thus, higher orders of matrix D will have sufficiently low condition number, and, more details of the x-ray spectrum of the device can be measured using the radiographic method. This explains why Raspa *et al* resolved the x-ray spectrum of a PF device into 15 components using the radiographic method [18].

5. Conclusion

A method for measuring the energy spectrum of an electron beam was presented and verified by the MCNP Monte Carlo code. This method is based on a matrix relation between the electron spectrum and the absorbed dose of the Bremsstrahlung photons, which are generated when the electron beam is stopped in a high Z target. The absorbed dose was measured using a radiography film and a set of lead filters with various thicknesses. This method is superior to other methods in terms of simplicity and cost, but a disadvantage of this method is the limited number of energy intervals or the poor resolution of the measured spectrum due to the error propagation problem.

The method was used for measuring the electron spectrum generated in a small PF device with 2.9 kJ energy, working at 0.6 mbar pressure of argon. The measured electron spectrum of the PF device at 0–500 keV shows that the electrons are most likely emitted in the 250–375 keV range. The probability of the emission of electrons with energies above 375 keV is very small, about 3% in this device. This is in line with the previous reports on the electron beam of the PF device. However, compared to other works, our method underestimates the spectrum at low energies.

References

[1] Lee P *et al* 1997 *Plasma Sources Sci. Technol.* **6** 343
[2] Tseng C H 2016 *Eur. J. Cancer* **61** 159
[3] Ceccolini E 2012 Development and performance assessment of a plasma focus electron beam generator for Intra-Operative Radiation Therapy *PhD* Bologna University, Italy
[4] Ceccolini E *et al* 2012 *J. Appl. Phys.* **112** 054901
[5] Pătran A C 2002 Electron and medium energy x-ray emission from a dense plasma focus *PhD* Nanyang Technological University, Singapore
[6] Neff W *et al* 1980 *Phys. Lett.* A **79** 165
[7] Neog N K and Mohanty S R 2007 *Phys. Lett.* A **361** 377
[8] Patran A *et al* 2005 *Plasma Sources Sci. Technol.* **14** 549
[9] Patran A *et al* 2006 *J. Fusion Energy,* **25** 57
[10] Ceccolini E *et al* 2011 *Rev. Sci. Instrum.* **82** 085103
[11] Kwiatkowski R *et al* 2011 *Nukleonika* **56** 119
[12] Zhang T *et al* 2006 *AIP Conf. Proc.* **808** 235
[13] Zhang T *et al* 2007 *Plasma Sources Sci. Technol.* **16** 250
[14] Khan I A *et al* 2010 *Nucl. Instrum. Methods Phys. Res.* B **268** 2228
[15] Wang Z P *et al* 2008 *Phys. Lett.* A **372** 7179
[16] Mather J W 1971 Dense plasma focus *Methods in Experimental Physics* (New York: Academic) pp 187–249
[17] Pavez C *et al* 2012 *Plasma Phys. Control. Fusion* **54** 105018
[18] Raspa V and Moreno C 2009 *Phys. Lett.* A **373** 3659
[19] Raspa V *et al* 2010 *Phys. Lett.* A **374** 4675
[20] Kanani A *et al* 2014 *Radiat. Phys. Chem.* **101** 59
[21] Surala W 2016 Research on electron beams and x-ray radiation in plasma-focus facilities *PhD* National Center for Nuclear Research, Poland
[22] Surala W *et al* 2016 *Nukleonika* **61** 161

[23] Sadowski M *et al* 1984 *Phys. Lett.* A **105** 117
[24] Jakubowski L and Sadowski M J 2002 *Brazil. J. Phys.* **32** 187
[25] Smith J R *et al* 1985 *Phys. Fluids* **28** 2305
[26] Styger W *et al* 1982 *Nucl. Fusion* **22** 1161
[27] Pouzo J *et al* 2002 *Eur. Phys. J.* D **21** 97
[28] Choi P *et al* 1988 *Phys. Lett.* A **128** 80
[29] Choi P *et al* 1990 *Laser Part. Beams* **8** 469
[30] Schneider R F, Rhee M J and Smith J R 1985 *IEEE Trans. Nucl. Sci.* **32** 3536
[31] Noll R *et al* 1983 *Phys. Lett.* A **99** 435
[32] Khan M Z 2016 Studies of x-ray and electron beam emissions from a low energy plasma focus *PhD* University of Malaya, Malaysia
[33] van Paassen H L L, Vandre R H and White R S 1970 *Phys. Fluids* **13** 2606
[34] Tartari A *et al* 2004 *Nucl. Instrum. Methods Phys. Res.* B **213** 206
[35] Gorbics S G and Pereira N R 1993 *Rev. Sci. Instrum.* **64** 1835
[36] Burden R L and Faires J D 2011 *Numerical Analysis* 9th edn (Boston, MA: Cengage Learning Publishing) pp 471–6